Chapter 4
Observation and Modeling of Cone Cracks in Ceramics

Brady Aydelotte and Brian Schuster

Abstract Ceramics undergo a complex failure process when subjected to impact by a projectile. Projectile impacts on thick ceramic targets produce varying levels of comminution, cone cracking, and radial cracking. Sphere impacts result in limited penetration and comminution relative to projectiles with a longer aspect ratio, yet significant radial and cone cracking is produced, and it is similar to Hertzian indentation. Sphere impact is a good way to study ceramics and a good validation problem to study the ability of hydrocodes to predict the formation and extent of radial and cone fractures in ceramic materials. Experimental results from normal and oblique sphere impacts on hot-pressed boron carbide cylinders are reported. Oblique sphere impacts created curved cone cracks, which did not appear oriented perpendicular to the impact surface. Cone angles appear to be the same for normal and oblique impacts for the impact conditions tested. Hydrocode predictions captured some but not all of the experimentally observed features.

Keywords Cone crack • Impact • Indentation • Ceramic • Damage

4.1 Introduction

Damage due to normal impact on ceramics has received considerable attention (see for example [1–6]). Evidently less effort has been directed towards the study of damage resulting from oblique impacts, particularly how it differs from damage resulting from normal impacts on armor grade ceramics. The terminology used in this paper to discuss different types of damage in a ceramic target from projectile impact is shown in Fig. 4.1. We could not find any published literature on oblique impact of ceramics, though there do exist some sliding indentation studies on polycrystalline ceramic materials [7–9]. Some work has also been done on oxide glasses [10–12].

In order to address this deficiency and further the study of the mechanical behavior of ceramics, we conducted impact experiments to explore the effects of oblique impacts on ceramics. We compared the cone cracking induced by normal and oblique impacts from tungsten carbide spheres on hot-pressed boron carbide (PAD B_4C) targets.

4.2 Experimental Setup

PAD B_4C cylinders 38.1 mm (1.5 in) diameter × 25.4 mm (1.0 in) length were procured from BAE Advanced Ceramics which is now owned by Coorstek. Some properties for PAD B_4C are listed in Table 4.1 for the reader's benefit.

The ceramic cylinders were impacted with 6.35 mm diameter (0.25 in) tungsten carbide-6 % cobalt (WC) spheres. Impact experiments were conducted at three different obliquities: 0°, 30°, and 60° from horizontal. Foam target holders were machined to orient the ceramic cylinders with an accuracy of plus or minus one degree. The spheres were fired out of a 0.30 caliber smooth-bore laboratory powder gun using plastic, two-piece, discarding sabots. WC projectile velocities were limited to between 200 and 500 m/s with emphasis on 300, 350, and 400 m/s impact velocities. The experimental setup is diagrammed in Fig. 4.2.

Two orthogonal pairs of 150 kV flash X-rays were used to determine projectile velocity. Additional 150 kV flash X-rays were used to capture late time (>100 μs post impact) images of fractures within the B_4C targets. The targets were recovered for future analysis. All angles were measured using FIJI [14] with repeated measurements to assess error.

B. Aydelotte (✉) • B. Schuster
US Army Research Laboratory, RDRL-WML-H321 Colleran Road, Aberdeen Proving Ground, MD 21005, USA
e-mail: brady.b.aydelotte.civ@mail.mil

B. Song et al. (eds.), *Dynamic Behavior of Materials, Volume 1*,
Conference Proceedings of the Society for Experimental Mechanics Series, DOI 10.1007/978-3-319-22452-7_4

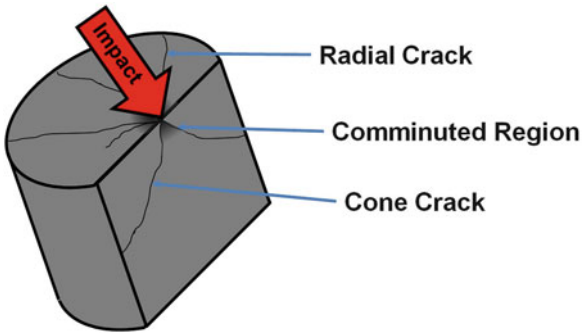

Fig. 4.1 Schematic of the damage produced by projectile impact on a thick cylindrical ceramic target showing our terminology for cone cracks, radial cracks, and a comminuted region. Comminution is the process of microcrack formation and intersection that converts a brittle solid into a granular material

Table 4.1 Selected mechanical properties of hot-pressed (PAD) B_4C from Vargas-Gonzalez et al. [13]

Density	Elastic modulus	Knoop hardness (HK2)	Fracture toughness
2.50 kg/m^3	445.5 GPa	2019 $\pm$ 60 kg/mm^2	2.90 $\pm$ 0.4 MPa$\sqrt{m}$

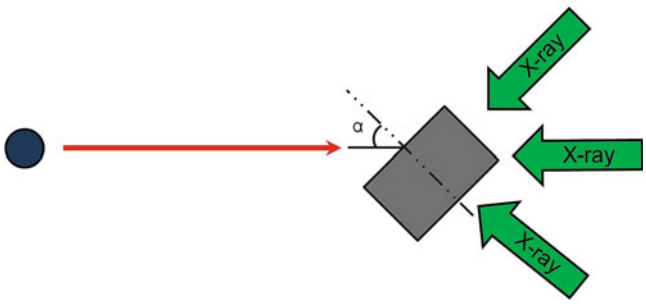

Fig. 4.2 Schematic of the impact experiments showing the obliquity measurement

4.3 Experimental Results and Analysis

Some selected results of the sphere impacts are shown in Fig. 4.3 for roughly three different velocities: 300, 350, and 400 m/s. There was considerable velocity scatter because it was difficult to hit low velocities with our current laboratory gun setup.

Cone cracks which form as a result of normal impacts are axisymmetric (unless the impact is off-center). Near the impact surface, the cone angle is constant. Away from the impact surface near the cylindrical sides of the target, the cone crack curves out to be normal to the sides of the cylinder. This is evident in Fig. 4.3a, d, g and is consistent with the PAD B_4C images published by LaSalvia et al. [4].

Cone cracks which form as a result of oblique impacts have concave down curvature on the leading edge and concave up curvature on the trailing edge. This behavior is evident in the oblique impacts in Fig. 4.3, and it is also shown schematically in Fig. 4.4. The curvature of cone cracks due to oblique impacts was also observed by Chaudhri and Liangyi [10] in soda-lime glass. We believe this is a result of cone crack surfaces locally reorienting themselves due to the spatially and temporally varying stress field from the projectile and/or debris sliding along the surface, changing the location of the maximum pressure. Chaudhri and Liangyi [10] also concluded that the movement of the point of contact was the cause of the curved cone cracks they observed in soda-lime glass. There may also be some effect from applying a shear load to the surface, though Chaudhri and Liangyi [10] didn't believe this effect was significant.

LaSalvia et al. [4] reported sphere impacts on PAD B_4C at 103, 209, and 312 m/s. The cone angles for the cone cracks in the targets impacted at 103 and 209 m/s measured 102°$\pm$ 2° and 82°$\pm$ 2° respectively. The outer cone of the PAD B_4C target impacted at 312 m/s measured 89°$\pm$ 2°, and the inner cone measured 31°$\pm$ 2°. The cone crack angles for the normal impacts reported in this work measured 78°$\pm$ 3°, 80°$\pm$ 3°, and 86°$\pm$ 3° for impacts at 284, 363, and 415 m/s respectively. This somewhat consistent with measurements of LaSalvia et al. [4] cone crack angles for impacts at 209 and 312 m/s.

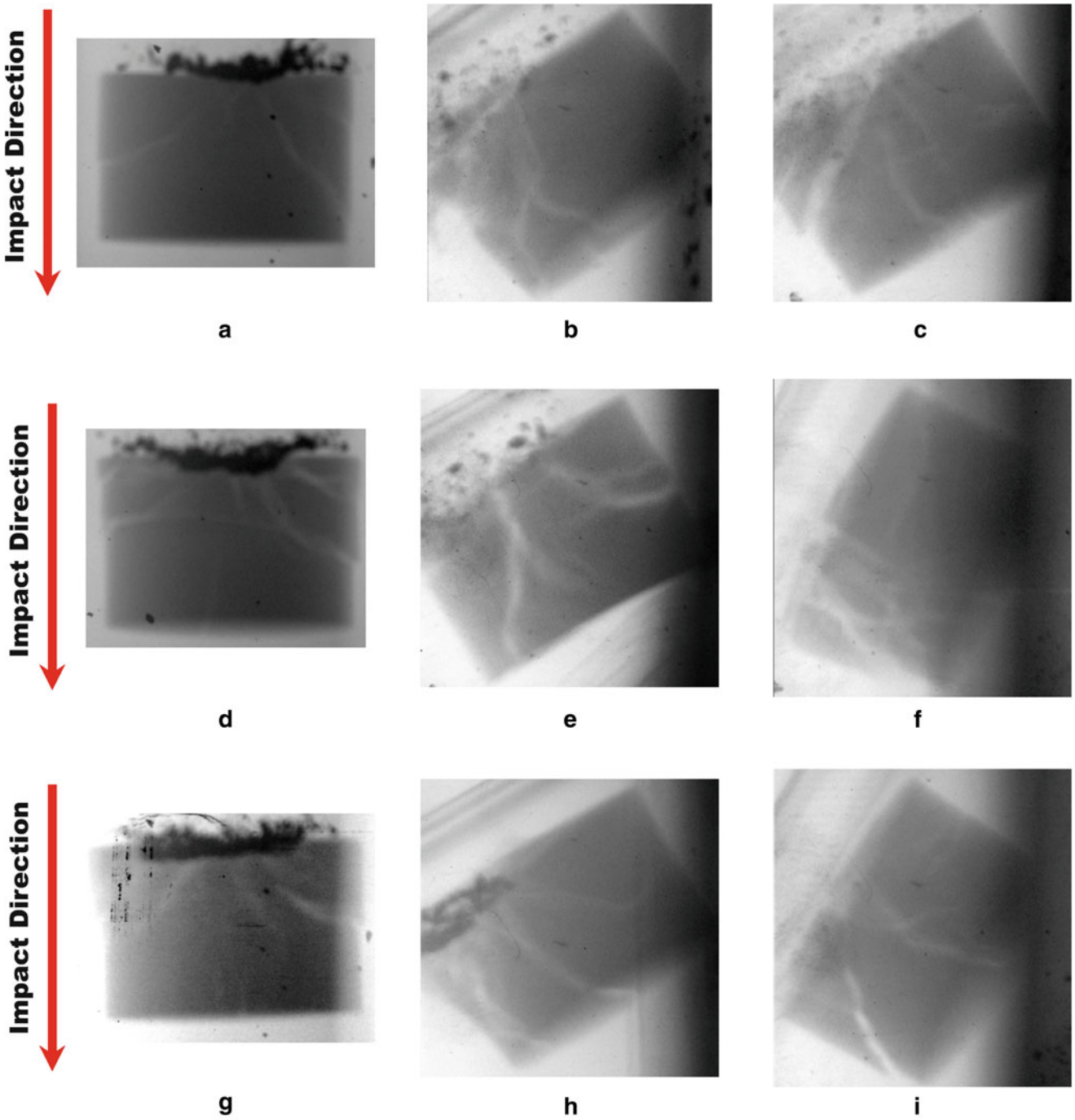

Fig. 4.3 Collected results of normal and oblique sphere impacts. Note that (**c**) is a 30° obliquity target. No 60° obliquity X-rays were captured around 300 m/s impact velocity. (**a**) V_{imp}: 284 m/s Obliquity: 0° Cone Angle: 78 ± 3°, (**b**) V_{imp}: 291 m/s Obliquity: 30° Cone Angle:? (**c**) V_{imp}: 310 m/s Obliquity: 30° Cone Angle: 78 ± 3°, (**d**) V_{imp}: 363 m/s Obliquity: 0° Cone Angle: 80 ± 3°, (**e**) V_{imp}: 392 m/s Obliquity: 30° Cone Angle: 82 ± 4°, (**f**) V_{imp}: 404 m/s Obliquity: 60° Cone Angle:?, (**g**) V_{imp}: 415 m/s Obliquity: 0° Cone Angle: 86 ± 3°, (**h**) V_{imp}: 431 m/s Obliquity: 30° Cone Angle: 75 ± 5°, (**i**) V_{imp}: 422 m/s Obliquity: 60° Cone Angle: 73 ± 5°

The oblique impacts which had measurable cone angles are shown in Fig. 4.3c,e,h,i. All had cone angles close to those measured for the normal impacts and roughly similar to those measured from the images in LaSalvia et al. [4]. Cone angle doesn't appear to be altered by target obliquity.

Nested cone cracks are commonly observed in impacts on ceramic targets with sufficient velocity. Most of the target X-rays in Fig. 4.3 show evidence of nested cone cracks; Nested cone cracks resulting from oblique impacts also tend to show

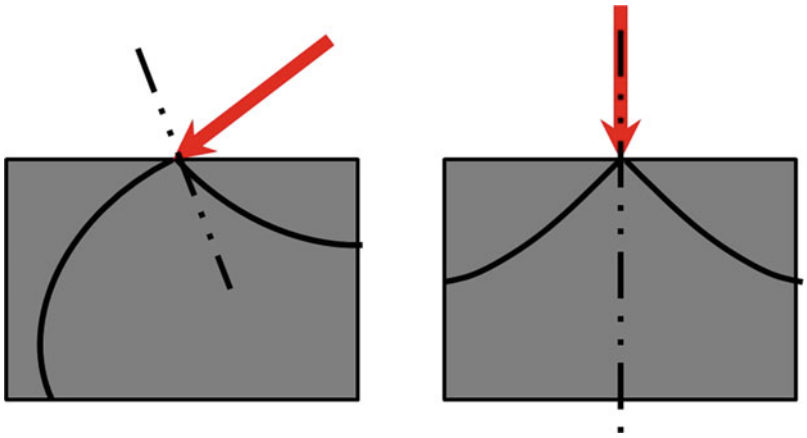

Fig. 4.4 Difference in cone orientation and shape for an oblique and normal impact respectively on a cylindrical ceramic target

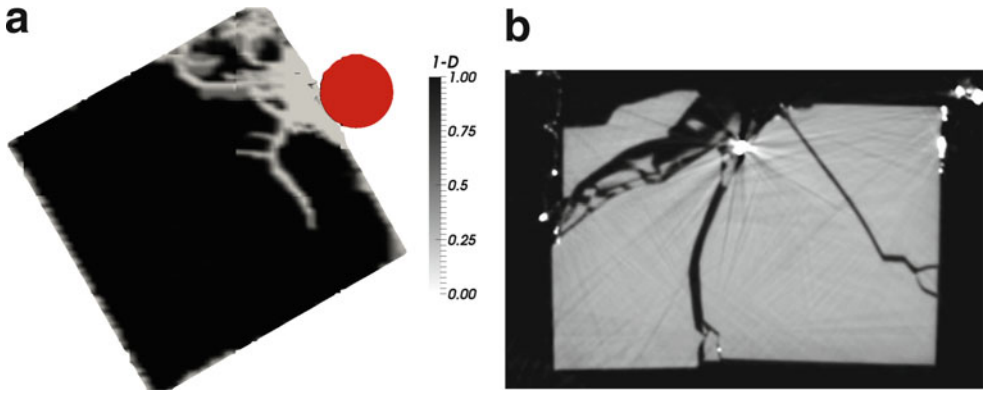

Fig. 4.5 (**a**) Simulated tungsten carbide sphere striking a B_4C cylinder target at an obliquity of 60°, 20 μs post-impact. Damaged ceramic appears white and undamaged ceramic appears black. The trailing portion of the cone crack is convex up and is similar to that seen in experiments. (**b**) Image produced by X-ray computerized tomography (CT) of a recovered target impacted at 310 m/s (also shown in Fig 4.3c). Note that the top of the cone crack is near the surface of the target, rather than a large region of comminuted material. The bright spots are tungsten carbide fragments which are embedded in the ceramic or in the foam target holder. The lines emanating from the tungsten carbide fragments are image artifacts from the tungsten carbide blocking X-rays inside the CT scanner as it revolved around the sample.

the curvature typical of oblique impacts. Figure 4.3e shows an interesting case where the outer cone crack is roughly symmetric, measuring 82°± 4° and the inner cone crack shows the concave down leading edge and the concave up trailing edge. The inner cone crack measures 46°± 3°.

4.4 Numerical Modeling

Preliminary efforts were made to model the sphere impact problems to gain greater insight into the evolution of damage and the development of cone cracks. A tungsten carbide sphere striking a boron carbide target at 300 m/s was modeling using the ALEGRA hydrocode [15]. The tungsten carbide sphere was modeled as elastic. Boron carbide was modeled with the KAYENTA geomaterial model [16].

The model accurately predicted the formation of the convex up region of the trailing end of the cone crack seen in Fig. 4.5a. The model didn't correctly predict the convex down region of the leading edge of the cone crack and it over-predicted the size of fully damaged regions underneath the sphere as seen in Fig. 4.5a,b. The differences between the model prediction and the impacted targets suggest that under the projectile, high hydrostatic compression results in very high strength in the boron carbide. This implies that our parameterization of the KAYENTA model could be reasonably adjusted to allow for higher strength at high pressure. This will be the subject of further investigation.

4.5 Conclusions

Sphere impacts on oblique ceramic targets have received no attention. Oblique impacts of this sort are similar to the classical Hertzian contact problem, but have the additional feature of some shear load applied on the surface as well as a changing center of maximum applied load. These additional features lead to substantial differences in the shape of the resulting cone cracks, but no apparent change in cone crack angle close to the impact surface. Hydrocode modeling of the impact was able to predict some of the features observed in experiments, the concave up trailing edge of the cone crack, but not the concave down leading edge of the cone crack.

Acknowledgements The authors acknowledge the helpful comments of Brian Leavy (ARL) and his assistance with the KAYENTA material model for boron carbide, Debjoy Mallick, and the ALEGRA development team at Sandia National Laboratory. We also acknowledge Cyle Teal (ARL) for his work on the 10 flash X-ray system, the laboratory technicians at ARL for assisting in these experiments, and the Department of Defense High Performance Computing Modernization Program for a grant of processing time.

References

1. Wilkins, M.L.: Mechanics of penetration and perforation. Spec. Issue: Penetration Mech. **16**(11), 793–807 (1978)
2. Shockey, D.A., Marchand, A., Skaggs, S., Cort, G., Burkett, M., Parker, R.: Failure phenomenology of confined ceramic targets and impacting rods. Int. J. Impact Eng. **9**(3), 263–275 (1990)
3. LaSalvia, J.C., Normandia, M.J., Miller, H.T., Mackenzie, D.E.: Sphere impact induced damage in ceramics: I. Armor-Grade SiC and TiB2. In: Advances in Ceramic Armor: A Collection of Papers Presented at the 29th International Conference on Advanced Ceramics and Composites, January 23–28, 2005, Cocoa Beach, Florida. Ceramic Engineering and Science Proceedings, pp. 170–181. Wiley, Hoboken, NJ, USA, (2005)
4. LaSalvia, J.C., Normandia, M.J., Miller, H.T., Mackenzie, D.E.: Sphere impact induced damage in ceramics: II. Armor-Grade B4c and WC. In: Advances in Ceramic Armor: A Collection of Papers Presented at the 29th International Conference on Advanced Ceramics and Composites, January 23–28, 2005, Cocoa Beach, Florida. Ceramic Engineering and Science Proceedings, pp. 183–192. Wiley (2005) Hoboken, NJ, USA
5. LaSalvia, J.C., Normandia, M.J., MacKenzie, D.E., Miller, H.T.: Sphere impact induced damage in ceramics: III. Analysis. In: Advances in Ceramic Armor: A Collection of Papers Presented at the 29th International Conference on Advanced Ceramics and Composites, January 23–28, 2005, Cocoa Beach, Florida. Ceramic Engineering and Science Proceedings, pp. 193–202. Wiley (2005) Hoboken, NJ, USA
6. LaSalvia, J., Leavy, R., Houskamp, J., Miller, H., MacKenzie, D., Campbell, J.: Ballistic impact damage observations in a hot-pressed boron carbide. In: Advances in Ceramic Armor V: Ceramic Engineering and Science Proceedings Volume 30, Issue 5, 2009, vol. 30, pp. 45–55. Wiley (2009)
7. Chiang, S.-S., Evans, A.G.: Influence of a tangential force on the fracture of two contacting elastic bodies. J. Am. Ceram. Soc. **66**(1), 4–10 (1983)
8. Laugier, M.: The surface fracture of alumina under a sliding spherical indenter. J. Mater. Sci. Lett. **5**(3), 253–254 (1986)
9. Ren, L., Zhang, Y.: Sliding contact fracture of dental ceramics: principles and validation. Acta Biomater. **10**, 3243–3253 (2014)
10. Chaudhri, M., Liangyi, C.: The orientation of the Hertzian cone crack in soda-lime glass formed by oblique dynamic and quasi-static loading with a hard sphere. J. Mater. Sci. **24**, 3441–3448 (1989)
11. Salman, A., Gorham, D., Verba, A.: A study of solid particle failure under normal and oblique impact. In: 8th International Conference on Erosion by Liquid and Solid Impact, vol. 186–187, Part 1, pp. 92–98 (1995)
12. Grant, P., Cantwell, W., McKenzie, H., Corkhill, P.: The damage threshold of laminated glass structures. Int. J. Impact Eng. **21**, 737–746 (1998)
13. Vargas-Gonzalez, L., Speyer, R.F., Campbell, J.: Flexural strength, fracture toughness, and hardness of silicon carbide and boron carbide armor ceramics. Int. J. Appl. Ceram. Technol. **7**(5), 643–651 (2010)
14. Schindelin, J., Arganda-Carreras, I., Frise, E., Kaynig, V., Longair, M., Pietzsch, T., Preibisch, S., Rueden, C., Saalfeld, S., Schmid, B., et al.: Fiji: an open-source platform for biological-image analysis. Nat. Methods **9**, 676–682 (2012)
15. Robinson, A.C., Carroll, S.K., Drake, R.R., Hansen, G.A., Hensinger, D.M., Kramer, R., Labreche, D.A., Love, E., Luchini, C.B., Mosso, S.J., et al.: ALEGRA User Manual. No. SAND2014-16031 (2014)
16. Brannon, R., Fossum, A., Strack, O.: Kayeta: Theory and User's Guide. No. SAND2009-2282 (2009)